DOI: 10.13009/EUCASS2017-625

Comparison of extensional and flexural modes for the design of piezoelectric ice protection systems

*Pierrick Rouset *, Marc Budinger** and Valérie Pommier-Budinger**
**ISAE SUPAERO, Institut Supérieur de l'Aéronautique et de l'Espace*
10 avenue Edouard Belin, 31400, Toulouse, France
*** Toulouse University, Institut Clément Ader (CNRS), INSA Toulouse*
3 rue Caroline Aigle, 31400, Toulouse, France

Abstract

Many researches focus on piezoelectric ice protection systems with the objectives to develop light and low consumption electromechanical systems for de-icing. These systems use vibrations, generated by the excitation of flexural, extensional or coupled resonance modes, to produce tensile stresses in the ice or shear stresses at the interface ice/support in order to remove ice. The objectives of this work are to analyse flexural and extensional resonance modes according to important design drivers for this type of systems: resonance frequency range, generation of tensile and shear stresses, electromechanical coupling factor, damping and fracture propagation. A final comparison gives pro and cons of each mode type for each design drivers for helping the designer of piezoelectric ice protection systems.

1. Introduction

1.1 State of the art on piezoelectric ice protection systems

Ice accretion on aircraft in flight can lead to lift decrease, drag increase, thrust reduction, risk of stalling or even engine failure owing to ice ingestion. These conditions can happen when the air contains humidity in the form of super cooled water droplets. Many systems have been implemented today on airplane using hot air from engines, pressure into deformable leading edge or heating electric devices. All of these systems consume a lot of energy and require maintenance. Some others devices like electro-impulse de-icing have been more recently introduced. Nevertheless, they required heavy actuators and power supply that limit their interest. An interesting alternative is to use the resonance frequencies of the iced structure in order to reduce the actuator size and the power consumption. These frequencies can be excited by piezoelectric actuators. Compared to other electromechanical actuators like voice coils, these actuators present the advantage to allow generation of vibrations on a very large bandwidth. A lot of research have studied two main resonance mode types: extensional corresponding to in plane displacements [1..6] and flexural corresponding to out of plane displacements [7..9]. The resonance frequency of these modes has been observed from low frequency (several Hz) [12..17] to medium (kHz) [1..9] or high frequency (MHz) [10][11]. Most of these studies show interesting experimental results by removing ice on all or part of the support. However, the ice fracture understanding is not yet well acquired and the mode type, the frequency range, the de-icing mechanisms are not yet fully compared and explained in order to optimize the system.

1.2 Objectives of the study

The global objective of our research project is to complete the existing studies [1]...[19] by identification of the main physical mechanisms and design drivers involved during the de-icing by piezoelectric devices. In order to ensure the ability to de-ice, an electromechanical ice protection system must be able not only to initiate fractures in the ice or at interface ice/support but also to propagate them. To design efficient resonant ice protection systems enabling fracture initiation, the resonance frequencies of each mode type need to be analyzed according to:
- the ability for generating the minimum tensile or shear stresses which can lead to the initiation of fractures (cracks with tensile stress and delamination with shear stress)
- the vibration amplitudes allowing to reach these stresses. The supply voltage and power required for generating these displacements depend on the damping of the structure.

DOI: 10.13009/EUCASS2017-625

- the electromechanical coupling factor between the structure with the ice and the actuator which is an indicator of the ability of the system to convert electrical energy in a useful way.

Once the frequencies are analyzed for enabling fracture initiation, the second step in the design of efficient resonant ice protection systems concerns the assessment of the resonance mode for propagating the fractures.

We can see that many parameters take part in the design process: resonance frequency range to generate tensile and shear stresses, electromechanical coupling factor, damping and fracture propagation. In this paper, our objective is to assess these significant parameters for their ability to initiate and propagate fractures for 2 types of resonance modes: extensional and flexural resonance modes.

1.3 Outlines of the study

This study relies on modelling and experimental results. The paper starts with an introduction of the modelling assumptions and of the test specimen used in the experiments. In section 3, flexural and extensional resonance modes that are both used in piezoelectric de-icing systems already experimented are studied: their frequency range is analysed, as well as the stresses and strains that they can develop. Then, in section 4, the force factor and electromechanical coupling factor are computed and analysed according to the types of modes. Section 5 focuses on the damping ratio and quality factor and highlights the differences between the flexural and extensional resonance modes. The issue of fracture propagation is addressed in section 6 through the analysis of experimental results. Finally the conclusion presents a comparison of each mode type with pro and cons for each design drivers.

2. Modelling assumptions and experimental setup

2.1 Ice mechanical properties

The ice characteristics are one of the first requirements to develop the de-icing system model. Ice mechanical properties are not always easy to estimate because there are several types of ice depending on the temperature and the size of the droplets. Furthermore, the ice is rarely perfectly homogeneous. Nevertheless, it is possible to distinguish three categories: glaze, mixed and rime ice. The glaze ice is formed at higher temperature (below 0°C) with a slow solidification speed which gives a transparent color to the ice. The rime ice freezes much faster at lower temperature or with smaller droplets. Air bubbles are trapped during icing process which gives a white color at this material. The ice elastic properties considered for different types of ice are presented in Table 1. These values come from data given in [20..24]. In this paper, the mechanical properties of glaze ice are considered for numerical and analytical simulation.

In addition to the elastic mechanical properties, the values of cohesive tensile strength and adhesive shear strength are necessary to predict the ice fractures. For our study, we consider the values of Table 2 issued from [20..25]. The values are high since our tests are performed in a freezer and not with atmospheric ice.

Table 1: Elastic mechanical properties of the glaze mixed and rime ice

	Glaze ice	Mixed ice	Rime ice
Young's modulus (GPa)	9.33	6.3	2.5
Poisson's ratio	0.33	0.33	0.28
Density (kg/m3)	917	800	600

Table 2: Tensile and adhesive shear strength of ice

	Freezer ice
Tensile strength (MPa)	3
Adhesive shear strength (MPa)	1

2.2 Analytical model assumption

In order to develop analytical analysis, the support with ice is considered as a thin multilayer beam (1D model). This section summarizes the equations already presented in previous works [19][26]. For more details on their assumptions and establishments, the reader can refer to the corresponding papers. Mode shapes are assumed to be identical to a uniform beam. Figure 1 shows the beam under study where:

- x is the transverse position over the beam of length a ;

DOI: 10.13009/EUCASS2017-625

- n is the number of anti-nodes for the considered mode ;
- ω is the pulsation of the considered mode ;
- h_{alu}, h_{ice}, h_n are respectively the thickness of the aluminum beam, the thickness of the ice beam and the position of the neutral line for the flexural mode,
- $U(x)$ and $W(x)$ are respectively the in-plane displacements (for extensional modes) and out-of-plane displacements (for flexural modes);
- c_{alu} , c_{ice} , ρ_{alu} and ρ_{ice} are respectively the Young' modulus and the density for the aluminum beam and the beam.

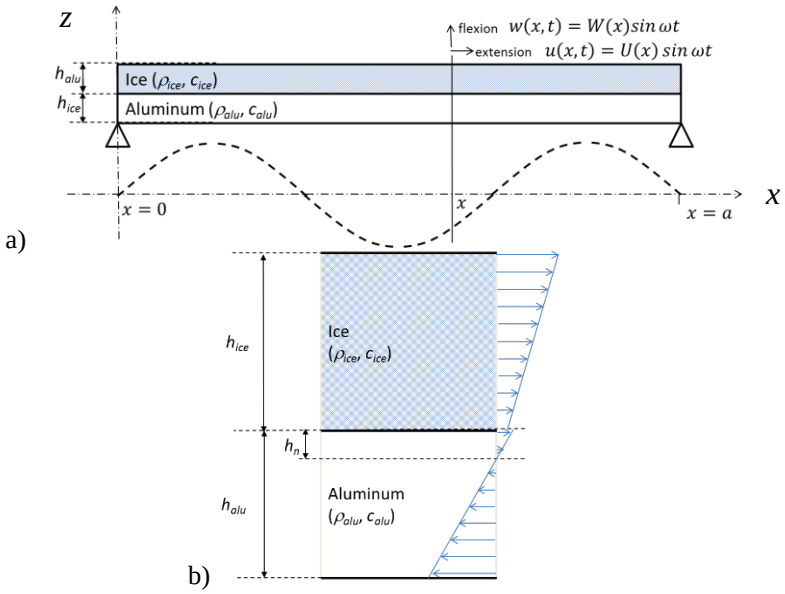

Figure 1: Element of the beam under study

For flexural modes, the position of the neutral line h_n can be obtained by assuming that the tensile force in a section is zero. This results in:

$$h_n = \frac{1}{2}\frac{c_{alu}h_{alu}^2 - c_{ice}h_{ice}^2}{c_{alu}h_{alu} + c_{ice}h_{ice}} \quad \textbf{(1)}$$

The beam is studied as a simply supported beam. Nevertheless, it will be shown (part 3.2) that the behavior is approximately the same for a free beam for the frequency range of our study (medium and high frequency).

2.3 De-icing test specimen

In order to conduct experimental tests, a specimen is configured. It consists of an aluminium plate of size 154x52x1.5 mm^3 with two ceramic bonded in the middle (Figure 2). One ceramic is used as a sensor and the other as an actuator. The sensor is symmetric to the actuator in order to analyse all the excited modes. The plate is tested with a constant ice layer formed in a freezer. The plate is hold with two nylon wires and the boundary conditions are considered as free. This configuration is not particularly optimised but the objective of the tests is here to excite the maximum of resonance frequency in order to test their efficiency for de-icing.

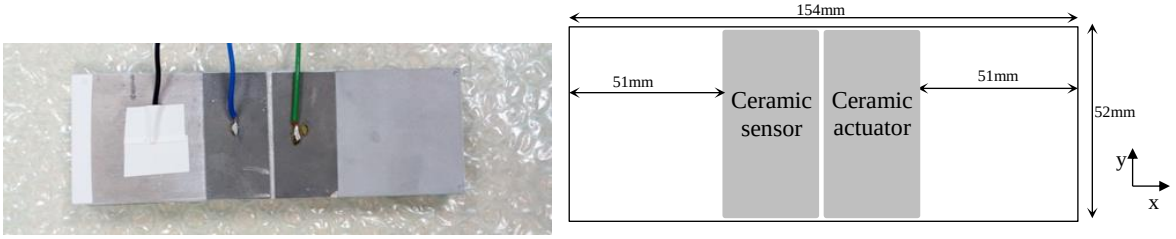

Figure 2: Test specimen: an aluminum plate with two ceramics bonded in the middle of the plate (one as a sensor, the other as an actuator)

DOI: 10.13009/EUCASS2017-625

3. Analysis of the frequency range and types of modes for initiating ice fractures

The purpose of this part is to understand how the fracture can be initiated in the ice depending on the frequency and the types of modes (flexural or extensional). The frequency range of the flexural and extensional modes is investigated here with the numerical model. The types of modes and their efficiency for the de-icing initiation are analysed with the analytical model that allows computing the stresses generated for all the resonance frequencies.

3.1 Frequency range of the flexural and extensional modes

A modal analysis of the modelled plate is firstly implemented with the finite element software Ansys© in order to report the different types of modes that can be excited and their frequency range. The study is performed from 100Hz to 50kHz, which corresponds to the frequency range of our electronic supply. The ice layer thickness is assumed to be constant and the numerical applications are made for 2mm. The computed mode shapes can be classified in two groups (Figure 3): the in-plane displacement modes as extensional modes and the out-of-plane displacement modes as flexural modes.

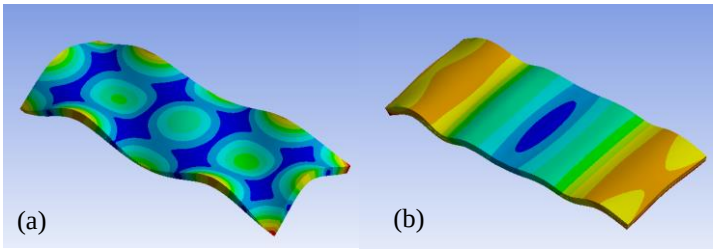

Figure 3: The two main mode types observed by modal analysis: flexural mode (a) and extensional mode (b)

The flexural mode can be composed of vibration nodes through the longitudinal or transversal axis or both (Figure 3.a). *n* is considered as the number of nodes in the longitudinal axis and *m* the number of nodes in the transversal axis.
The extensional modes considered here are only composed of nodes in the longitudinal axis. More complex extensional modes exist but they will not be studied here. *n* is considered as the number of nodes in the longitudinal axis (blue area in Figure 3.b). It is possible to notice that extensional modes do not generate only in-plane displacements. Out-of-plane displacements are also generated along the longitudinal axis. Figure 4 gives all the resonance frequencies for the extensional and flexural modes depending on their number of longitudinal and transversal nodes.
Figure 4 shows that the resonance frequencies increase with the number of nodes in transversal (m) or in longitudinal direction (n). Flexural modes exist for low frequencies (from less than 1 kHz) although extensional modes are present only above 15 kHz. For a given frequency range, extensional modes are less numerous than flexural modes.

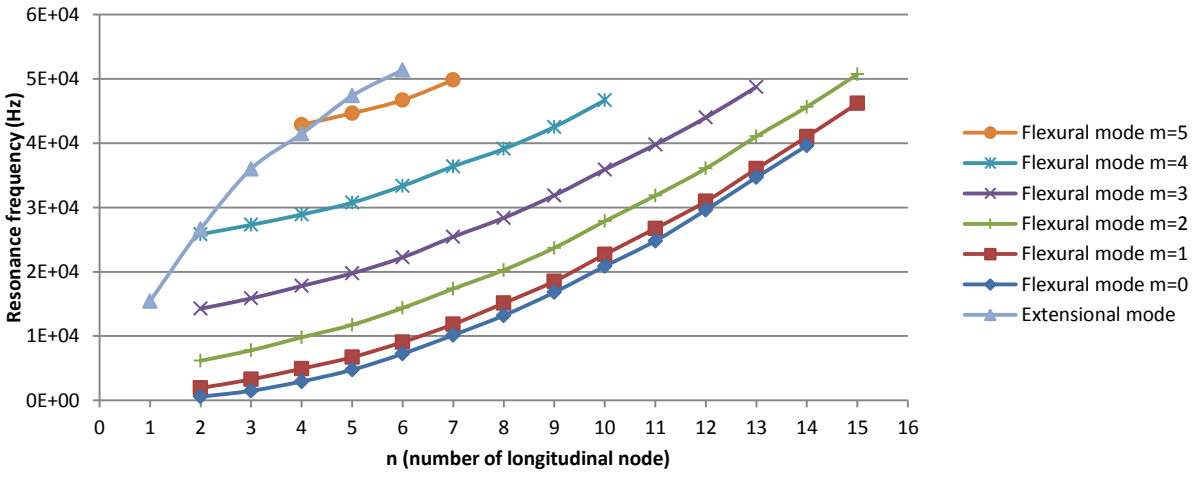

Figure 4: Resonance frequencies depending on the number of nodes in the longitudinal and transversal directions for the extensional and flexural modes (results from FEM analysis)

DOI: 10.13009/EUCASS2017-625

3.2 Developments and analysis of analytical models of stresses and strains for initiating ice fractures

To design a de-icing system, a strength criterion has to be implemented. Indeed, the ice should be sufficiently deformed to reach strengths that can detach ice accumulations on surfaces. Two mechanisms of fracture are possible: cracking in the ice layer due to tensile stress or delamination at the interface between the substrate and the ice due to shear stress (Figure 5).

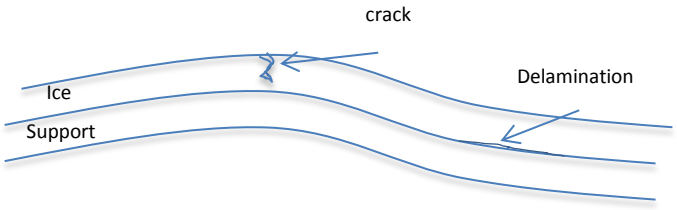

Figure 5: Cracking and delamination mechanisms due to the deformation of the ice and the support with the piezoelectric de-icing system.

In order to simplify the analytic models, the beam is considered as simply supported. This hypothesis is checked by the numerical model used previously. A free and a simply supported plate are implemented in Ansys© and the resonance frequencies depending on the number of longitudinal nodes are computed and presented in Figure 6. The two nodes generated by the simply supported boundary conditions are taken into account in the value of *n*.
An even node number corresponds to a symmetric mode which is not affected by the symmetric boundary conditions. The difference between the free and simply supported case is more visible for the anti-symmetric modes (13% of resonance frequency error for extensional modes and 6% for flexural modes). Nevertheless, the error is assumed to be negligible and the simple supported beam assumption is used to simplify the model.

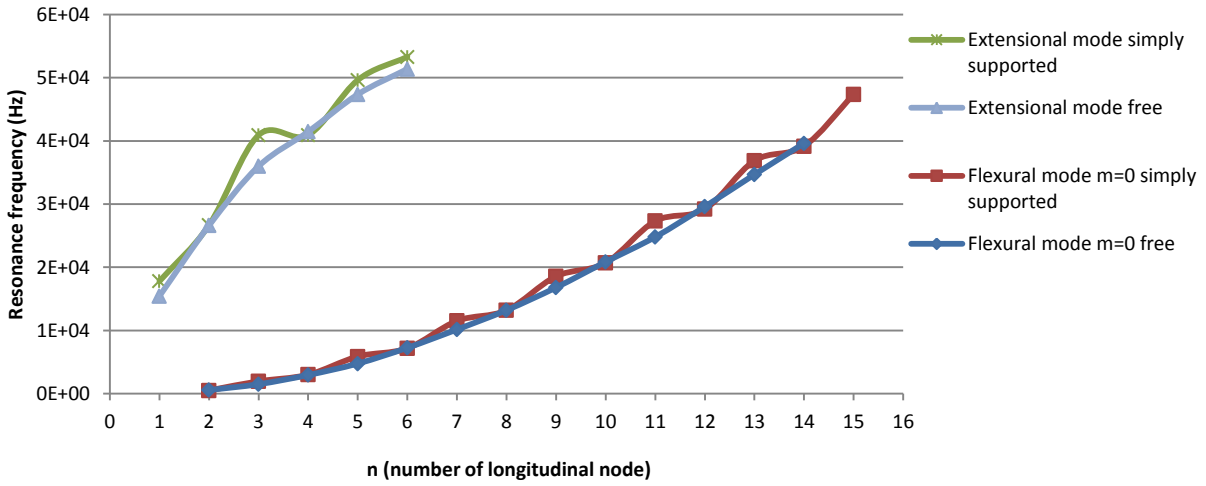

Figure 6: Resonance frequencies depending on the number of node in the longitudinal direction for the extensional and flexural mode with free and simply supported boundary conditions (results from FEM analysis).

Table 3 synthetizes the analytical formulas derived from previous assumptions to compute strains and stresses in the ice, in the aluminum support and at the interface ice/support. The formulas of the peak out-of-plane shear stress were obtained by isolating an element of ice of thickness *dx* subjected to elastic forces, inertial forces and shear forces at the interface ice/support. The resonance frequencies were obtained by Rayleigh method using the expression of the strains to estimate the kinetic and potential energies.

These formulas show that the tensile stress in the ice is maximal at the displacement nodes for extensional modes and at the displacement anti-nodes for the flexural modes. The maximum shear stress at the interface ice/support is located at the displacement node for the flexural mode and the displacement anti-node for the extension. This means that it is difficult to couple the two types of stress in the same zone if only one resonance mode is used.

DOI: 10.13009/EUCASS2017-625

Table 3: 1D modes formula for simply supported boundary conditions

	Extensional modes	**Flexural modes**
Displacement	$u(x,t) = U(x)\sin\omega t = U_0 \sin\frac{n\pi x}{a}\sin\omega t$	$w(x,t) = W(x)\sin\omega t = W_0 \sin\frac{n\pi x}{a}\sin\omega t$ $u(x,t) = -z\frac{\partial w}{\partial x} = -zW_0\frac{a}{n\pi}\cos\frac{n\pi x}{a}U(\sin\omega t)$
Peak tensile strain	$\varepsilon_x = \frac{\partial U(x)}{\partial x} = U_0\frac{n\pi}{a}\cos\frac{n\pi x}{a}$	$\varepsilon_x = \frac{\partial U(x)}{\partial x} = W_0 z\left(\frac{n\pi}{a}\right)^2 \sin\frac{n\pi x}{a}$
Peak tensile stress in ice	$\sigma_x = c_{ice}\varepsilon_x = c_{ice}U_0\frac{n\pi}{a}\cos\frac{n\pi x}{a}$	$\sigma_x = c_{ice}(h_{ice}+h_n)\left(\frac{n\pi}{a}\right)^2 W_0 \sin\frac{n\pi x}{a}$
Peak tensile stress in aluminum	$\sigma_x = c_{alu}\varepsilon_x = c_{alu}U_0\frac{n\pi}{a}\cos\frac{n\pi x}{a}$	$\sigma_x = c_{alu}(h_{alu}-h_n)\left(\frac{n\pi}{a}\right)^2 W_0 \sin\frac{n\pi x}{a}$
Peak out-of-plane shear stress at the interface ice/support	$\tau_{xz} = \left(\rho_{ice}\omega^2 - c_{ice}\left(\frac{n\pi}{a}\right)^2\right)h_{ice}U_0 \sin\frac{n\pi x}{a}$	$\tau_{xz} = c_{alu}\left(\frac{n\pi}{a}\right)^3 \frac{(h_{alu}-h_n)^2 - h_n^2}{2} W_0 \cos\frac{n\pi x}{a}$
Angular frequency	$\omega = \pi\frac{n}{a}\left(\frac{c_{ice}h_{ice}+c_{alu}h_{alu}}{\rho_{ice}h_{ice}+\rho_{alu}h_{alu}}\right)^{1/2}$	$\omega = \pi^2\left(\frac{n}{a}\right)^2\left(\frac{EI}{\rho_{ice}h_{ice}+\rho_{alu}h_{alu}}\right)^{1/2}$ with $EI = \frac{c_{alu}}{3}(h_n^3 + (h_{alu}-h_n)^3) + \frac{c_{ice}}{3}((h_n+h_{ice})^3 - h_n^3)$

The tensile strength and the adhesive shear strength given in Table 2 can be used in the formulas of the peak tensile stress in ice and of the peak out-of-plane shear stress at the interface formula (Table 4) to compute the amplitude W_0 and U_0 leading respectively to the initiation of delamination or cracking. The computed displacements are plotted according to the frequency in Figure 7. The flexural and extensional modes require much more displacements at low frequency than at high frequency. In fact the distance between anti-nodes at low frequency is longer and requires more displacement in order to generate the same bend radius than at high frequency and thus reached the same stresses. Furthermore, the amplitude leading to the initiation of fractures at fixed frequency is higher for extensional modes than for flexural modes, which means that flexural modes generate more stress in the ice for a given displacement. In order to minimize displacements and reduce consumption, it is more interesting to use flexural modes to initiate a delamination or fracture.

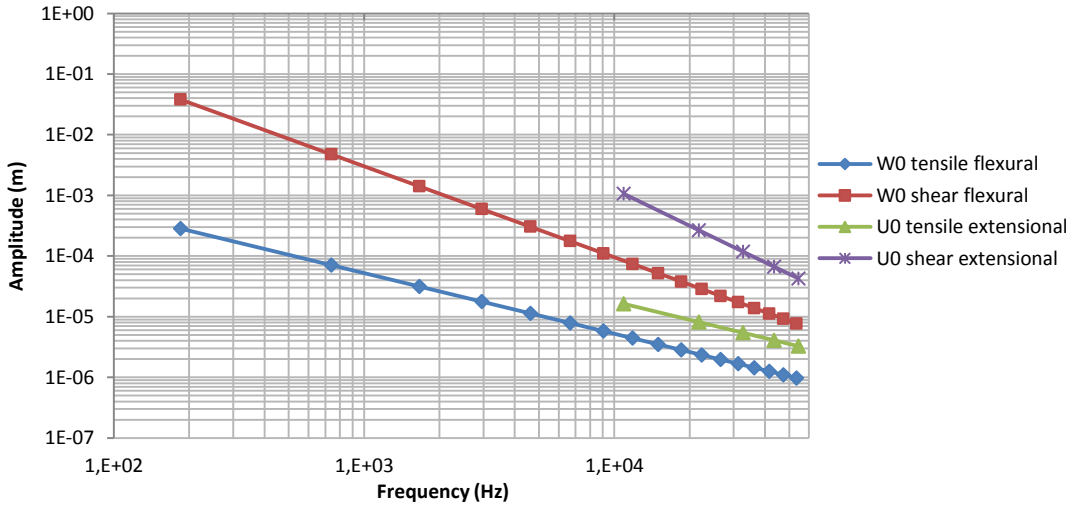

Figure 7: Amplitude required for initiating cracks in the ice or delamination at the interface ice/support according to the frequency for extensional and flexural modes

DOI: 10.13009/EUCASS2017-625

4. Force factor and electromechanical coupling factor

The objective of this part is to calculate the force factor and the electromechanical coupling factor in order to study the impact of the actuator size on the electromechanical conversion.

4.1 Piezoelectric and electromechanical equations

The local piezoelectric equations are defined as:

$$\begin{cases} \boldsymbol{T} = \boldsymbol{c}^{E}\boldsymbol{S} - \boldsymbol{e}\boldsymbol{E} \\ \boldsymbol{D} = \boldsymbol{\varepsilon}^{S}\boldsymbol{E} + \boldsymbol{e}^{t}\boldsymbol{S} \end{cases} \quad \textbf{(2)}$$

with $\boldsymbol{T}$ the stress vector, $\boldsymbol{E}$ the electric field vector, $\boldsymbol{D}$ the electric displacement field vector, $\boldsymbol{S}$ the strain vector, $\boldsymbol{c}^{E}$, $\boldsymbol{e}$ and $\boldsymbol{\varepsilon}^{S}$ the piezoelectric coupling matrices.
The reduced model of a structure with piezoelectric actuators comprises a mechanical equation and an electrical equation. The model presented here comes from [19]. The model reduced to one mode is written:

$$\begin{cases} M\ddot{q} + D_s\dot{q} + Kq = NV \\ q_C = Nq + C_o V \end{cases} \quad \textbf{(3)}$$

where q is the modal displacement, M the modal mass, K the modal stiffness, qc the electrical charge, V the voltage, D_s the modal damping, N the modal electromechanical coupling force factor, and C_o the modal turned-off capacity.
The force factor N is directly linked to the piezoelectric effects. In order to maximize the displacement with the minimum voltage, a mode with a high force factor is desired. The objective here is to calculate the force factor value for each mode type. This factor is estimated for a given point by using the second equation and calculating the electrical charge q_C on the electrodes for a zero voltage $V=0$ and the deformation q of the selected point.

4.2 Force factors

In order to simplify the computations, the geometries and ceramic positions of Figure 8 are assumed for the flexural and extensional modes. The calculations are done according one anti-node in free condition for the extensional mode and in antisymmetric condition for the flexural mode. The actuator is taken into account and the ceramic length is configurable along the x axes and constant along the y and z axis. The extensional mode is assumed to be only along the x axis and without parasitic flexural mode.

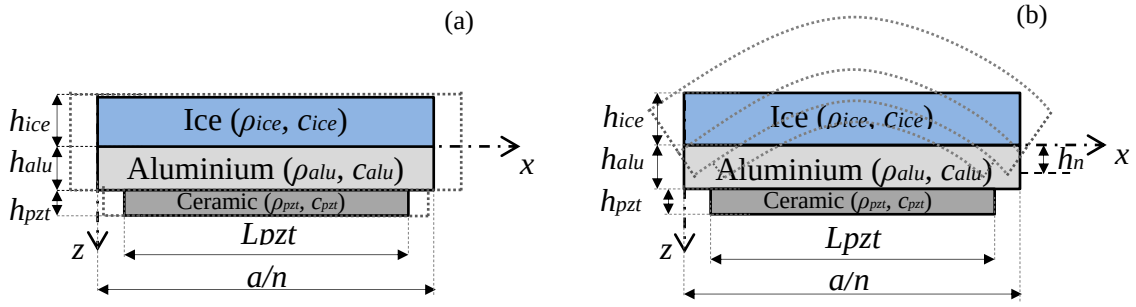

Figure 8: Simplified model for the force factor calculation: extensional mode (a) and flexural mode (b)

In this configuration, the electric displacement field and electric field vectors have only one non-zero component along y axis. It can be written here with scalar notation D and E. The electric field E into the ceramic cannot be assumed to be constant for a zero voltage according to the finite element simulation. It is possible to write $\partial D / \partial y = 0$ due to the absence of free charge thanks to Gauss theorem. In this way, the electric displacement field D is constant on the thickness of the ceramic but is function of the position x. D is thus egal to the average value along the y axis. The equation expressing D can be approximated by the following scalar equation:

$$D = \varepsilon^{S}E + eS \quad \textbf{(4)}$$

DOI: 10.13009/EUCASS2017-625

where $e = -\gamma e_{33} + (1-\gamma)e_{31}$ is the sum of e_{33} (strain along *y* axis) and e_{31} (strain along *y* axis) multiplied by γ (Poisson coefficient). The average of (4) in the thickness of the ceramic gives:

$$\langle D \rangle = D(x) = \varepsilon^S \langle E \rangle + e\langle S \rangle = \varepsilon^S \frac{V}{h_{PZT}} + e\frac{1}{h_{PZT}} \int_{h_{alu}-h_n}^{h_{alu}-h_n+h_{PZT}} s(x,y)dz \quad \textbf{(5)}$$

with h_{PZT} the thickness of the PZT ceramic.

The electric displacement field *D* becomes:

$$D_{ext}(x) = e\frac{n\pi}{a}U_0 \sin\frac{n\pi x}{a} \quad \textbf{(6)}$$

$$D_{flex}(x) = e\left(\frac{n\pi}{a}\right)^2 W_0 \left(\frac{h_{PZT}}{2} + h_a - h_n\right)\cos\frac{n\pi x}{a} \quad \textbf{(7)}$$

D_{ext} and D_{flex} the electric field displacement for extensional and flexural modes.

The integration of the electric displacement field on the ceramic surface gives the electrical charge allowing to estimate the force factor:

$$N_{ext} = \frac{q_c}{q} = 2eb\sin\frac{n\pi l_{pzt}}{2a} \quad \textbf{(8)}$$

$$N_{flex} = \frac{q_c}{q} = 2eb\left(\frac{n\pi}{a}\right)\left(\frac{h_{PZT}}{2} + h_a - h_n\right)\sin\frac{n\pi l_{PZT}}{2a} \quad \textbf{(9)}$$

with N_{ext} and N_{flex} the force factor of an extensional mode and a flexural mode.

It is now possible to represent, Figure 9, the force factor depending on the ratio between the actuator length and the length between anti-nodes (equations (8),(9)). Figure 9 shows that the force factor is maximum for a ratio of 1 when the actuator has the same length as the distance between two nodes (node to node length). Moreover, equations (8) and (9) show that the force factor for flexural mode increases with the number of nodes *n* while the force factor for the extensional mode is constant with *n*. The force factor of an extensional mode can be always considered as higher than for the force factor of a flexural mode. Nevertheless, it is not possible to conclude with the comparison of these two values because the force factor doesn't express the capacity of vibration generation on the same displacement. Figure 9 shows also that the force factor can be degraded if the length of the actuator is higher than node-to-node length. The Figure 10 shows the anti-node length according to the frequency and highlights for flexural modes the risks of underutilization of volume of ceramics at high frequency due to the small node to node length.

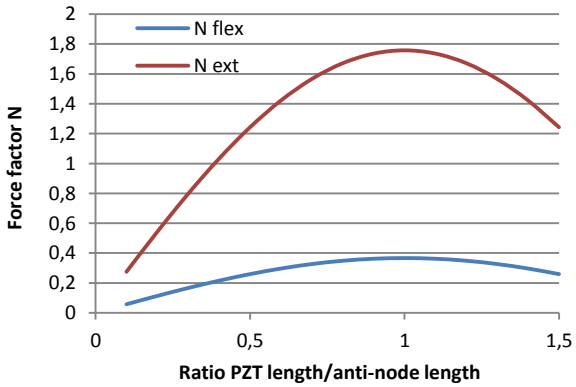

Figure 9: Force factor depending on the ceramic length for flexural and extensional mode for *n* =10

DOI: 10.13009/EUCASS2017-625

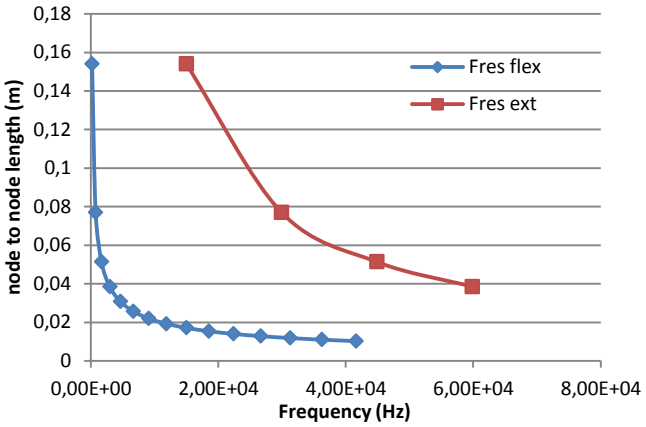

Figure 10: Node to node length according to the frequency for the plate under study

4.3 Electromechanical coupling factor

The electrical and mechanical equation given by (3) can be presented in the form of a diagram (Figure 11) which corresponds to the equivalent electric behaviour of a transducer defined by the simplified diagram *RLC//C*$_0$. In this diagram, *M* and *K* are the modal mass and the stiffness of the mode.

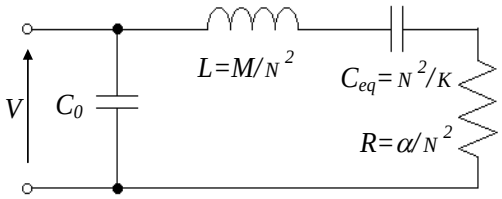

Figure 11: Equivalent electric scheme of a transducer [28]

The coupling factor can be defined as an energy ratio which expresses the ability to transform electrical energy into mechanical energy. As described in [28], the coupling factor of the ceramic can be defined as:

$$k^2 = \frac{1/C_0}{1/C_0 + 1/C_{eq}} = \frac{C_{eq}}{C_0 + C_{eq}} \quad \textbf{(10)}$$

with

$$C_0 = \frac{\varepsilon^S L_{PZT} b}{h_{PZT}} \quad \textbf{(11)}$$

$$C_{eq} = \frac{N^2}{K} \quad \textbf{(12)}$$

The stiffness can be obtained with the potential energy. The potential energy of the ceramic is considered as negligible. The potential energy U_i can be written as:

$$U_i = \iiint \frac{1}{2} TSdv = \iint \frac{1}{2} c \left(\frac{\partial U(x)}{\partial x} \right)^2 bdxdy \quad \textbf{(13)}$$

The potential energies for extensional modes (U_{ext}) and flexural modes (U_{flex}) are written as:

$$U_{ext} = \frac{1}{2}(c_{alu} h_{alu} + c_{ice} h_{ice}) \left(\frac{n\pi}{a} \right)^2 \frac{a}{2n} b U_0^2 \quad \textbf{(14)}$$

$$U_{flex} = \frac{1}{2} \left(\frac{c_{alu}}{3}(h_n^3 + (h_{alu} - h_n)^3) + \frac{c_{ice}}{3}(h_n + h_{ice})^3 - h_n^3) \right) \left(\frac{n\pi}{a} \right)^4 \frac{a}{2n} b W_0^2 \quad \textbf{(15)}$$

The stiffness for extensional modes (K_{ext}) and flexural modes (K_{flex}) are deduced from the expressions of potential energy:

DOI: 10.13009/EUCASS2017-625

$$K_{ext} = (c_{alu} h_{alu} + c_{ice} h_{ice}) \left(\frac{n\pi}{a}\right)^2 \frac{a}{2n} b \quad \textbf{(16)}$$

$$K_{flex} = \left(\frac{c_{alu}}{3}(h_n^{\,3} + (h_{alu} - h_n)^3) + \frac{c_{ice}}{3}(h_n + h_{ice})^3 - h_n^{\,3})\right)\left(\frac{n\pi}{a}\right)^4 \frac{a}{2n} b \quad \textbf{(17)}$$

Finally, the coupling factor can be obtained from equations (10), (11), (12) using the stiffness from equations (16)(17) and the force factor computed in the last section. The coupling factor is independent from frequency and plotted according to the ratio between the actuator length and the node to node length (Figure 12). The coupling factor seems to reach a maximum for a given ratio of actuator length by node to node length. In fact, if the actuator length corresponds to 0.7 times the node to node length, the coupling factor and thus the actuator efficiency is optimal for flexural and extensional modes. Furthermore, the coupling factor is higher for a flexural mode than an extensional mode which means that flexural mode is more efficient whatever the actuator length. Therefore, the flexural modes have a clear positive benefit in terms of coupling factor and energy conversion.

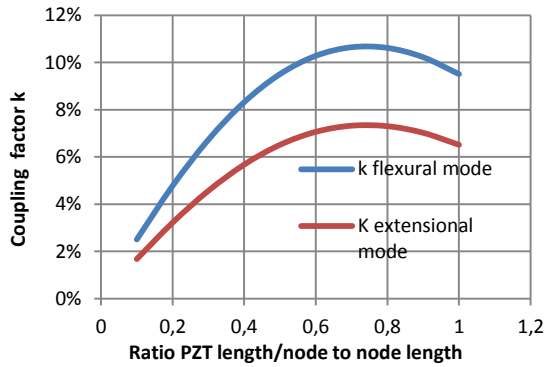

Figure 12: Coupling factor according to the ratio between the actuator length and the node to node length for flexural and extensional modes

5. Damping and quality factor

This section discusses on the damping ratio which is a characteristic of the structure that influences the voltage for supplying the actuator in order to obtain the required displacements for fracture initiation and propagation. The higher the damping ratio is, the higher the voltages of the actuators must be, and consequently the higher is the consumption.

5.1. Sources of damping

This part concerns the study of the different losses linked to the vibratory state of the plate. The extensional and flexural modes are compared in order to minimize the specific power needed to compensate the mechanical losses. Various causes can introduce damping in the structure. The sources of the mechanical loses are presented in Table 4 [29][30].

Table 4: Sources of the mechanical losses

Mechanical losses	**Source**
Viscous fluid losses	When vibrating in a fluid, a plate is perturbed by viscosity and mass density of the environment.
Acoustic losses	The vibration of the plate in the fluid creates an acoustic pressure which propagates into the fluid.
Support losses	The vibrations produce a mechanical work on the support and losses.
Thermo-elastic losses	Losses are caused by the material heating due to vibration.

DOI: 10.13009/EUCASS2017-625

Viscoelastic material	Polymers composed (glue) of long molecular chains have viscoelastic properties.
Micro-slipping and pumping effect	The dynamic forces which occur in structures whose jointed (or riveted) parts may slide or generate air pumping effect during dynamic loading are associated with energy dissipation.

The damping is mainly driven by support losses, thermo-elastic losses and viscoelastic material (possibly due to the glue). Viscous fluid losses and acoustic losses appear to be negligible with the studied geometry [31]. Furthermore, micro-slipping is considered as negligible and support losses are not considered here since the plate is in free conditions.

The damping is linked to the quality factor Q which expresses the vibration intensification at the resonance:

$$Q = \frac{(KM)^{1/2}}{D_s} \tag{18}$$

where M is the modal mass, K the modal stiffness and D_s the modal damping.
More generally, the quality factor is the ratio between the total energy stored due to the elastic deformation and the energy dissipated per cycle described as:

$$Q = 2\pi \frac{Total\,energy\,stored}{Energy\,\,dissipated\,\,per\,\,cycle} \tag{19}$$

5.2. Quality factor measurement

The parameter Q is interesting because it experimental value is simply evaluated with:

$$Q = \frac{f_{res}}{\Delta f_{-3dB}} \tag{20}$$

with Δf_{-3dB} the -3dB bandwidth and f_{res} the resonance frequency.
For our test specimen, the quality factor is thus measured for the different resonance frequencies available on the used frequency range. The experimental results are presented in Figure 13. It shows that the quality factors increase with the frequency. The quality factor for the extensional mode is approximately two to three times higher than flexural mode which means that the damping is much lower for the extensional mode. The measured quality factors are quite high because the tests are performed for a plate in free conditions. There are thus no losses in the support.

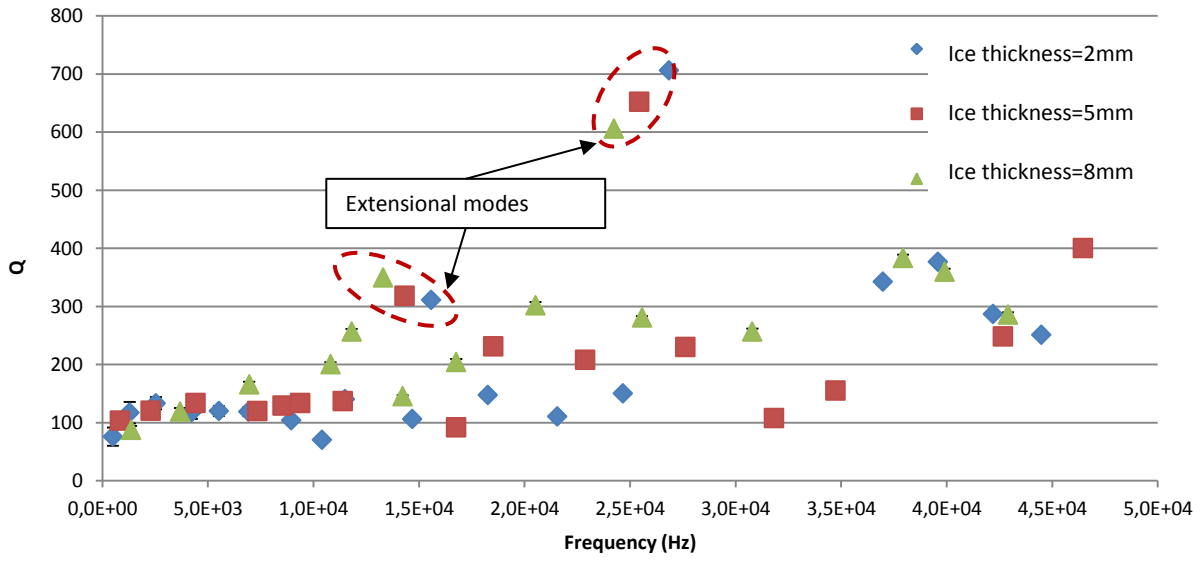

Figure 13: Experimental quality factor results depending on the frequency for different thickness

DOI: 10.13009/EUCASS2017-625

5.3 Analysis of quality factors

The global quality factor of a structure composed of several parts can be estimated, for a mode, knowing :

- the quality factor of the material of each part (in our case: Q=1000 for the ice, Q=1000 for the aluminum, Q=25 for the piezoelectric actuator in PIC151 and Q=10 for the epoxy glue)
- the elastic energy U_i of each part that can be computed with a modal analysis of FEM software,

and using the formula:

$$Q = \frac{\sum U_i}{\sum \frac{U_i}{Q_i}} \tag{21}$$

The difference in the quality factors can be easily explained by the difference of the elastic energy repartition in flexural and extensional modes. Figure 14 shows that the elastic energy in the piezoelectric ceramic is larger, compared to the other parts of the structure, for flexural modes than for extensional modes. Indeed, for flexural modes, the ceramic is far from the neutral line and its strain is thus important. As the piezoelectric material has a low quality factor compared to the other material, if it has a relative high elastic energy, relation (21) shows that the quality factor of the structure is low.

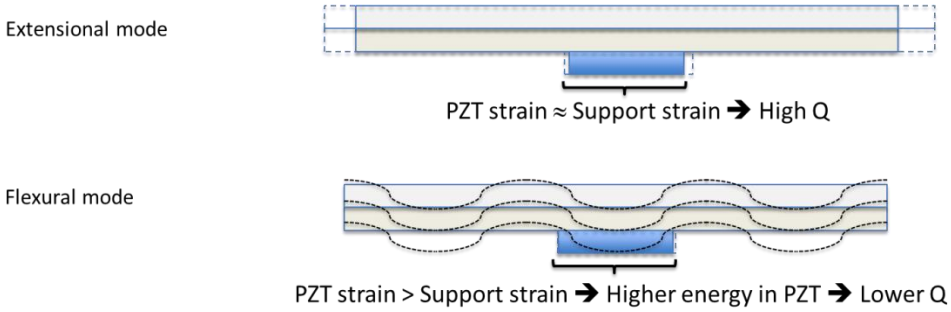

Figure 15: Explanation of the difference of quality factor between flexural and extensional mode

6. Experimental results concerning fracture propagation

Figure 7 shows that the tensile strength is reached before the shear strength for flexural and extensional modes. Consequently, cracks are more likely to appear first in the de-icing process. Once the cracks are initiated, the question arises if they propagate or not in the ice and if they can be followed by delamination at the interface ice/support. In this last section, experimental results for three resonance modes of the plate under study are presented to observe what happens after the crack initiation (Figure 16). For the two flexural modes, only cracks are observed. For the mode at 15kHz with in-planes and out-of-planes displacements, cracks and delamination can be observed. The modal analysis performed to study the plate, shows that elastic energy stored in this mode is more important than for the flexural modes. This allows a propagation of the cracks through the ice and delamination of the interface ice/support with the same vibratory amplitude as the one computed to initiate the fracture, without any extra energy.

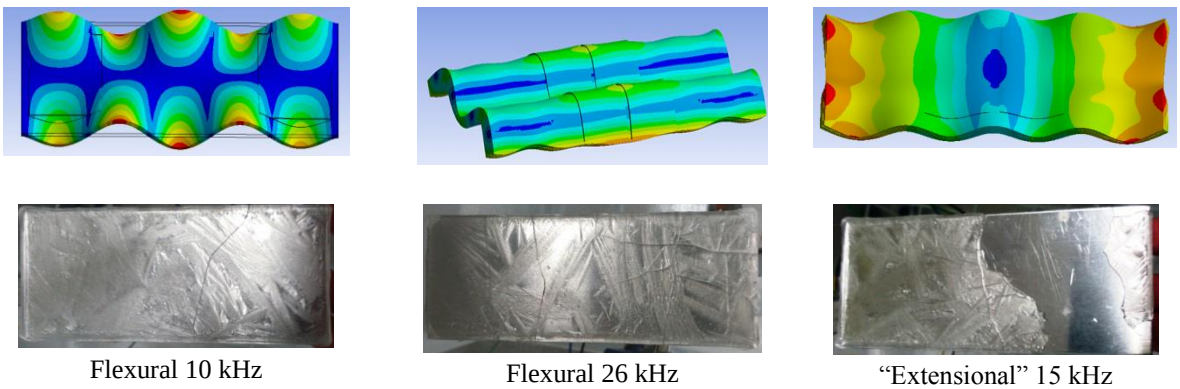

Flexural 10 kHz | Flexural 26 kHz | "Extensional" 15 kHz

Figure 16: Experimental tests

DOI: 10.13009/EUCASS2017-625

7. Comparison and conclusion

This article has proposed to analyze important features to be taken into account for the design of resonant piezoelectric ice protection systems. Using analytical and numerical models, as well as experimental tests results, flexural and extensional resonance modes that are used to generate vibrations and stresses in the ice or at the interface ice/support were analyzed according to: resonance frequency range, generation of tensile and shear stresses, electromechanical coupling factor, damping and fracture propagation. Table 5 summarizes the main results concerning these criteria. It shows that flexural modes are interesting in terms of frequency bandwidth, to work at low frequencies, for generation of tensile and shear stress and to obtain a good electromechanical coupling. On another side, the extensional modes, which are very present in the ultrasonic frequency bandwidth, have higher force factor, lower damping and can initiate and propagate the fractures with the same level of energy. Recommending the use of a particular mode is still difficult. The idea that comes to mind is to couple the use of these two modes in order to exploit their respective advantages.

Table 5: Advantages and drawback of each mode depending on the criteria studied

Criteria	Flexural modes	Extensional modes
Frequency range	☺ Large frequency range ☹ Noisy if under 20 kHz	☹ Few resonance modes often higher than 20 kHz ☺ Silent tests
Tensile and shear stress generation	☺ Generate more easily tensile and shear stress at given frequency	☹ Need more displacements to generate stresses
Electromechanical coupling	☺ Best coupling factor	☺ High force factor with high frequency (ceramic size)
Damping		☺ Best quality factor
Energy for fracturation		☺ Best fracturation

References

[1] Palacios, J. L., Design, Fabrication, and Testing of an Ultrasonic De-icing System for Helicopter Rotor Blades, Ph.D Thesis, The Pennsylvania State University, Department of Aerospace, May 2008.

[2] Palacios, J. L., Smith, E. C., Rose, J., "Investigation of An Ultrasonic Ice Protection System For Helicopter Rotor Blades," Annual Forum Proceedings - AHS International 64th Annual Forum, Vol. 64, No. 1, 2008, pp. 609–618.

[3] Palacios, J. L., Smith, E. C., Rose, J., Royer, R., "Ultrasonic De-icing of Wind Tunnel Impact Icing," Journal of Aircraft, Vol. 48, No. 3, 2011, pp. 1020–1027.

[4] Palacios, J. L., Smith, E. C., "Dynamic Analysis and Experimental Testing of Thin-Walled Structures Driven by Shear Tube Actuators," 6 th AIAA/ASME/ASCE/AHS/ASC Structures, Structural Dynamics, and Materials Conference, 2005, p. 1-14.

[5] Overmeyer, A., Palacios, J., Smith, E., Royer, R., Rotating Testing of a Low-Power, Non-Thermal Ultrasonic De-icing System for Helicopter Rotor Blades, SAE Technical Paper, International Conference on Aircraft and Engine Icing and Ground De-icing, Chicago, IL, No. 2011-38-0098, June 2011.

[6] Overmeyer, A., Palacios, J., Smith, E., "Actuator Bonding Optimization and System Control of a Rotor Blade Ultrasonic De-icing System," 53rd AIAA/ASME/ASCE/AHS/ASC Structures, Structural Dynamics and Materials Conference 20th AIAA/ASME/AHS Adaptive Structures Conference 14th AIAA, 2012, p. 1476.

[7] Strobl, T., Storm, S., Kolb, Thompson, D., Hornung, M., Thielecke F., Tobias Strobl, "Feasibility Study of a Hybrid Ice Protection System", Journal of Aircraft, Vol. 52, No. 6 (2015), pp. 2064-2076.

[8] Strobl, T., Storm, S., Kolb, M., Haag, J., & Hornung, M. (2014, September). Development of a Hybrid Ice Protection System Based on Nanostructured Hydrophobic Surfaces. In 29th Congress of the International Council of the Aeronautical Sciences.

[9] Villeneuve, E., Harvey, D., Zimcik, D., Aubert, R., & Perron, J. (2015). Piezoelectric De-icing System for Rotorcraft. Journal of the American Helicopter Society, 60(4), 1-12.

[10] Ramanathan, S., Varadhan, V. V., Varadhan, V. K., De-icing of Helicopter Blades Using Piezoelectric Actuators, Smart Structures and Materials, Smart Electronics and MEMS, SPIE's 7th Annual International

DOI: 10.13009/EUCASS2017-625

Symposium on Smart Structures and Materials. International Society for Optics and Photonics, 2000, pp. 281-292.
[11] Kalkowski, M. K., Waters, T. P., Rustighi, E., "Removing Surface Accretions with Piezo-Excited High-Frequency Structural Waves," Proc. SPIE 9431, Active and Passive Smart Structures and Integrated Systems 2015, San Diego, California, March 2015.
[12] Venna, S. V., Lin, Y. J., "In-Flight De-icing Self-Actuating Wing Structures with Piezoelectric Actuators," Proceedings of American Society of Mechanical Engineers/International Mechanical Engineering Congress and Exposition 2002, ASME Press, New York, 2002, pp. 237–245.
[13] Venna, S. V., Lin, Y. J., "Development of Self-Actuating In-Flight De-icing Structures with Power Consumption Considerations," Proceedings of the American Society of Mechanical Engineers International Mechanical Engineering Congress and Exposition 2003, ASME Press, New York, 2003, pp. 45–53.
[14] Venna, S. V., Lin, Y. J., "Mechatronic Development of Self-Actuating In-Flight De-icing Systems," IEEE/ASME Transactions on Mechatronics, Vol. 11, No. 5, 2006, pp.585–592.
[15] Venna, S. V., Lin, Y. J., Botura, G., "Piezoelectric Transducer Actuated Leading Edge De-icing with Simultaneous Shear and Impulse Forces," Journal of Aircraft, Vol. 44, No. 2, 2007, pp. 509–515.
[16] Palacios, J., Smith, E., Rose, J., Royer, R., "Instantaneous De-icing of Freezer Ice via Ultrasonic Actuation," AIAA Journal, Vol. 49, 2011, No. 6, pp. 1158–1167.
[17] Struggl, S., Korak, J., Feyrer, C., A Basic Approach for Wing Leading De-icing by Smart Structures, Sensors and Smart Structures Technologies for Civil, Mechanical, and Aerospace Systems, Vol. 7981, 2011, p. 79815L-79815L-10.
[18] Endres, M., Sommerwerk, H., Mending, C., Sinapius, M., Horst, P. (2016). Experimental study of two mechanical de-icing systems applied on a wing sction tested in an icing wind tunnel
[19] Budinger, M., Pommier-Budinger, V., Napias, G., & Costa da Silva, A. (2016). Ultrasonic Ice Protection Systems: Analytical and Numerical Models for Architecture Tradeoff. Journal of Aircraft, (0), 680-690
[20] Gammon, P. H., Kiefte, H., Clouter, M. J., & Denner, W. W. (1983). Elastic constants of artificial and natural ice samples by Brillouin spectroscopy. Journal of Glaciology, 29(103), 433-460.
[21] Eskandarian, M. (2005). Ice shedding from overhead electrical lines by mechanical breaking (Doctoral dissertation, Ph. D. thesis, University of Quebec at Chicoutimi).
[22] Mohamed, A. M. A., & Farzaneh, M. (2011). An experimental study on the tensile properties of atmospheric ice. Cold regions science and technology, 68(3), 91-98.
[23] Gao, H., & Rose, J. L. (2009). Ice detection and classification on an aircraft wing with ultrasonic shear horizontal guided waves. IEEE transactions on ultrasonics, ferroelectrics, and frequency control, 56(2), 334-344.
[24] Nakaya, U. (1958). Visco-elastic properties of snow and ice in Greenland ice cap. Journal of the Faculty of Science, Hokkaido University. Ser. 2, Physics= 北海道大學理學部紀要 5(3), 119-164.
[25] Druez, J., Phan, C. L., Laforte, J. L., & Nguyen, D. D. (1979). The adhesion of glaze and rime on aluminum electrical conductors. Transactions of the Canadian Society for Mechanical Engineering, 5(4), 215-220.
[26] Pommier-Budinger, V., Budinger, M., Tepylo, N., & Huang, X. (2016). Analysis of piezoelectric ice protection systems combined with ice-phobic coatings. In 8th AIAA Atmospheric and Space Environments Conference (p. 3442).
[27] Ikeda, T., Fundamentals of Piezoelectricity, Oxford Science Publications.
[28] Budinger, M. (2003). Contribution à la conception et à la modélisation d'actionneurs piézoélectriques cylindriques à deux degrés de liberté de type rotation et translation (Doctoral dissertation, Institut National Polytechnique de Toulouse-INPT).
[29] F. Lochon, I. Dufour, D. Rebière, Microcantilever chemical sensors optimization by taking into account losses, Sensors and Actuators B 118 (2006) 292–296.
[30] Groper, Meshulam. "Microslip and macroslip in bolted joints." Experimental Mechanics 25.2 (1985): 171-174.
[31] Zoghaib, L., & Mattei, P. O. (2015). Damping analysis of a free aluminum plate. Journal of Vibration and Control, 21(11), 2083-2098.